An Electrochemical Quartz Crystal Microbalance Investigation of Manganese Oxide Deposition and Dissolution in Sulfuric Acid Relevant for Zinc Electrowinning

S. M. Skaftun[a], S. Sunde[a], G. M. Haarberg[a], and F. Seland[a]

[a] Department of Materials Science and Engineering, Norwegian University of Science and Technology (NTNU), NO-7491 Trondheim, Norway

The deposition and dissolution of manganese oxide from a sulfuric acid solution were investigated by conventional electrochemical techniques and EQCM on gold and platinum electrodes. The product of the oxidation was found by EQCM to be MnO_2 at a higher potential (1.55 V), whereas a mixture between MnOOH and MnO_2 was produced at a lower potential (1.45 V). An ECE mechanism involving the formation of MnOOH was proposed as the oxidation mechanism. A higher deposit porosity was obtained at the higher deposition potentials. The reduction mechanism was proposed to involve an electrochemical reduction of MnO_2 to MnOOH, followed by a chemical reaction yielding Mn^{2+} and MnO_2.

Introduction

Deposition of manganese dioxide have been extensively studied for battery and supercapacitor applications. In these applications, the manganese oxide is typically deposited in an acidic electrolyte, but operated in neutral or alkaline solutions. In neutral or alkaline solution manganese oxide can exist in a number of different oxidation states, according to the Pourbaix diagram (1), and the electrochemical behavior could differ significantly from that in acidic environments. In addition to the number of oxidation states that can occur in manganese oxides, the tetravalent manganese dioxide (MnO_2) that is encountered in acidic solution exists in a number of polymorphs (2).

Manganese dioxide deposition is also relevant in aqueous metal electrowinning processes such as zinc electrowinning, where deposition occurs on the anode as a side reaction to the oxygen evolution reaction (OER). There are several differences between the deposition conditions for MnO_2 in zinc electrowinning and for production of battery materials. The temperature is much lower in zinc electrowinning (~35 °C), the electrolyte is more acidic (~2 M H_2SO_4) and the Mn^{2+}-concentration could be lower (varies). The manganese dioxide deposit causes several problems in zinc electrowinning and the removal of the deposit is therefore of interest, especially when employing an anode that is catalytically active for OER.

Several authors have discussed the mechanism of manganese dioxide deposition and dissolution in acid, and a number of different (and parallel) routes have been suggested (2). Paul and Cartwright (3, 4) demonstrated that during the formation of MnO_2, a relatively stable and poorly conducting intermediate is formed on the outer surface of the growing deposit. They argued that the rate of deposition is limited by the diffusion of manganese ions through this intermediate to oxidize it to MnO_2. An ECE mechanism involving the formation of MnOOH was suggested by Petitpierre *et al.* (5):

$$Mn^{2+} \rightarrow Mn^{3+} + e^- \qquad\qquad [1]$$

$$Mn^{3+} + 2H_2O \rightarrow MnOOH + 3H^+ \qquad\qquad [2]$$

$$MnOOH \rightarrow MnO_2 + H^+ + e^- \qquad\qquad [3]$$

The same authors also suggested that at high temperatures the Mn^{3+} could disproportionate and form MnO_2 in the bulk of the electrolyte according to reactions [4] and [5], as observed by Welsh (6).

$$2Mn^{3+} \rightarrow Mn^{2+} + Mn^{4+} \qquad\qquad [4]$$

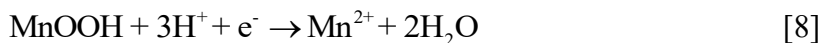$$Mn^{4+} + 2H_2O \rightarrow MnO_2 + 4H^+ \qquad\qquad [5]$$

The mechanisms of formation and reduction is dependent on the acid strength, the concentration of manganese in the solution and the temperature (7). The Mn^{3+}-ion has an enhanced stability at low pH (8). The oxidation mechanism of Mn^{2+} has thus been suggested to involve a competition between the two pathways presented above (9): the hydrolysis mechanism given by Eqs. [1]-[3] which is favored at high pH and the disproportionation mechanism given by Eqs. [1], [4] and [5] at low pH.
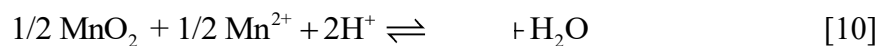
A mechanism for the reduction of electrodeposited MnO_2 was proposed by Lee $et\ al.$ and Maskell (10-12):

$$MnO_2 + H^+ + e^- \rightarrow MnOOH \qquad\qquad [6]$$

$$2MnOOH + 2H^+ \rightleftharpoons \qquad + Mn^{2+} + 2H_2O \qquad\qquad [7]$$
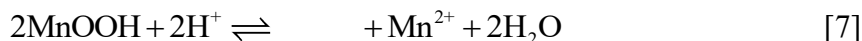
They found that the reduction proceeds in two peaks with a third peak appearing at high acid strengths. The first peak was found to be independent on electrode material, whereas the second peak depended very much on the electrode material. Both the first and second peak were suggested to follow the reaction scheme above. After the first peak, the crystal structure was found to be unaltered, whereas the conductivity had decreased. The decrease in conductivity was explained by an increase in contact resistance resulting from the volume reduction caused by the reaction. They also suggested that a blocking Schottky-type barrier was formed at the interface between the semiconducting MnO_2 and the substrate. This required a larger overpotential for the continued reduction and resulted in a second peak. Bodoardo $et\ al.$ (13) also presumed the same pathway. Similarly, the reduction of MnO_2 was explained by proton insertion in a cation vacancy model by Ruetschi (14). Accordingly, a change in crystal structure upon reduction of MnO_2 through Eq. [6] is not expected, as MnOOH and MnO_2 are isomorphic (15).

Other possible reactions parallel to or following reaction [6] have been suggested (11, 16, 17):

$$MnOOH + 3H^+ + e^- \rightarrow Mn^{2+} + 2H_2O \qquad\qquad [8]$$

$$MnOOH + 3H^+ \rightleftharpoons \qquad - 2H_2O \qquad\qquad [9]$$

$$1/2\ MnO_2 + 1/2\ Mn^{2+} + 2H^+ \rightleftharpoons \qquad + H_2O \qquad\qquad [10]$$

$$Mn^{3+} + e^- \rightarrow Mn^{2+} \qquad\qquad [11]$$

To try to distinguish between the different mechanisms, *in situ* techniques can be employed to obtain additional information about the processes. For instance, Raman spectroscopy has been employed to distinguish between MnOOH and Mn(OH)$_2$ during the reduction of MnO$_2$ in alkaline electrolyte (18). The electrochemical quartz crystal microbalance (EQCM) can be used to provide additional information about the mass change during deposition and dissolution of manganese dioxide. Dupont and Donne (9) used EQCM to show that the increase in mass when oxidizing Mn^{2+} in an acidic electrolyte was an intermediate between those expected from MnOOH and MnO$_2$ formation (based on the charge). However, in that work only one deposition potential was applied. EQCM has been employed to study the deposition and/or dissolution of manganese dioxide in sulfuric acid solutions in other works as well (19-21). However, these works mainly concern the production of manganese dioxide for supercapacitors, and does not necessarily focus on the reduction of the deposit or the voltammetric behavior. The aim of this work is to study manganese oxide deposition and dissolution from a sulfuric acid solution using conventional electrochemical methods and EQCM.

Experimental

Electrochemical Quartz Crystal Microbalance (EQCM)

The EQCM measurements were performed using Metrohm Autolab's EQCM module and cell (polypropylene). The EQCM crystals were 6 MHz AT-cut crystals with 100 nm thick platinum or gold electrodes and a 10 nm TiO$_2$ adhesion layer (International Crystal Manufacturing, part number 151717-6 and 151527-6 respectively). The crystal diameter was 13.6 mm and the electrode diameter was 6.7 mm. The measured frequency change was related to the mass change using the Sauerbrey equation (22):

$$\Delta f = \frac{-2 f_0^2 \Delta m}{A \left(\mu_q \rho_q \right)^{1/2}} = -C_f \frac{\Delta m}{A} \qquad\qquad [12]$$

where Δf is the measured change in frequency, f_0 the frequency of the quartz crystal prior to mass change, Δm the mass change, A the piezoelectric active area, C_f the sensitivity factor, ρ_q the density and μ_q the shear modulus of quartz.

The crystals were cleaned prior to electrochemical measurements by immersion in a heated, acidified (0.18 M H$_2$SO$_4$) solution of 10 wt% H$_2$O$_2$ for a brief time (less than 1 minute). After the immersion, the crystals were rinsed with copious amounts of de-ionized water (MilliQ, 18.2 MΩ cm) and dried under nitrogen atmosphere.

Electrochemical Measurements

Conventional electrochemical measurements were performed using an Autolab PGSTAT302N potensiostat. The electrolyte consisted of 0.1 M H$_2$SO$_4$ (VWR Chemicals, AnalaR Normapur) with or without 5 mM MnSO$_4$ (Merck, pro analysi) and was prepared

using de-ionized water (MilliQ, 18.2 MΩ cm). The electrolyte was deaerated prior to the experiments by purging with Ar-gas (AGA, 5.0). During the experiments the argon outlet was placed directly above the electrolyte surface. All experiments were carried out at room temperature (22 °C ± 0.5 °C). A reversible hydrogen electrode (RHE) was used as a reference electrode and all potentials are reported versus this electrode. A gold wire served as the counter electrode. The cell contained 3 mL electrolyte in the EQCM experiments. The working electrodes were preconditioned by repeatedly cycling them at 100 mV/s in 0.1 M H_2SO_4 for 100 cycles prior to the electrochemical measurements. In the chronoamperometry experiments, the initial potential was 1.1 V on platinum electrodes to ensure that the metal oxide layer had already formed and did not contribute significantly to the measured current after the step. In the case of the gold electrode, the initial potential was set to 0.5 V as the onset of gold oxide formation overlaps with that of manganese oxide formation.

In addition to the EQCM experiments, chronoamperometry was performed on platinum discs (geometric area 0.785 cm^2) in a 0.1 M H_2SO_4 + 5 mM $MnSO_4$ electrolyte using a large three-electrode glass cell (1000 mL). The purpose of these experiments was to obtain manganese dioxide deposits at selected time intervals and potentials, and to study them with scanning electron microscopy (SEM). In this work, the platinum electrodes were held for 100 s, 1000 s and 10 000 s at 1.45 and 1.55 V. The potentials were chosen based on the results from cyclic voltammetry.

Scanning Electron Microscopy (SEM)

A scanning electron microscope (Hitachi S-3400N) was used to examine manganese oxide deposits formed by chronoamperometric methods as described in the previous paragraph. After each deposition experiment, the electrode was removed from the cell and rinsed with de-ionized water before being left to dry. After imaging, the platinum disc was polished using 0.3 μm and 0.05 μm alumina paste in order to remove residual manganese oxide, before being rinsed with de-ionized water.

Results and discussion

Cyclic Voltammetry

Gold and platinum electrodes were examined by cyclic voltammetry and EQCM in sulfuric acid with and without Mn^{2+}-ions as illustrated in Figure 1. Metal oxides were formed on both electrodes in acid, starting from about 0.8 V on platinum and 1.4 V on gold, as seen in Figure 1a. The metal oxides were completely reduced in the negative-going sweep, in a reduction wave peaking at around 0.7 V on platinum and 1.2 V on gold. The massograms (Figure 1b and d) showed a weight increase during metal oxide formation and a corresponding weight loss during the metal oxide reduction peaks. The onset of OER was visible before potential reversal at 1.6 V on platinum at the sweep rate of 5 mV/s, but negligible on the gold electrode. The peaks close to the lower reversal potential in the Pt voltammogram are related to hydrogen underpotential deposition and desorption. The voltammograms and massograms in Figure 1 are similar to those reported in the literature (23, 24).

Upon addition of manganese ions to the electrolyte several new peaks appeared, as can be seen in Figure 1c), where the features are similar on both substrates. An oxidation peak is clearly visible in the positive-going sweep just below 1.5 V ($p_{ox,1}$) followed by the onset of oxygen evolution, visible for the Pt electrode at the upper reversal potential. The oxidation peak in the positive-going sweep ($p_{ox,1}$) is not related to oxygen evolution as it occurs prior to the onset of oxygen evolution on both electrodes and coincides with the onset of a significant mass increase (Figure 1d).

Initially, the current remains positive after reversing the potential sweep leading to a, somewhat surprisingly, second oxidation peak ($p_{ox,2}$) at potentials slightly negative of 1.5 V, coinciding with the oxidation peak in the positive-going sweep ($p_{ox,1}$). It is worth noticing the slight change in slope of the massograms occurring at about 1.5 V in both the positive-going and negative-going sweep directions indicating a faster mass increase at the lower potentials. This appears to imply an activation of the surface at these potentials.

During the negative-going sweep, the current becomes negative at a potential of about 1.40 V, at which the mass peaks, with two main reduction peaks, $p_{red,1}$ at 1.3 V and $p_{red,2}$ negative to the first reduction peak. Both reduction peaks are accompanied by a significant decrease in mass.
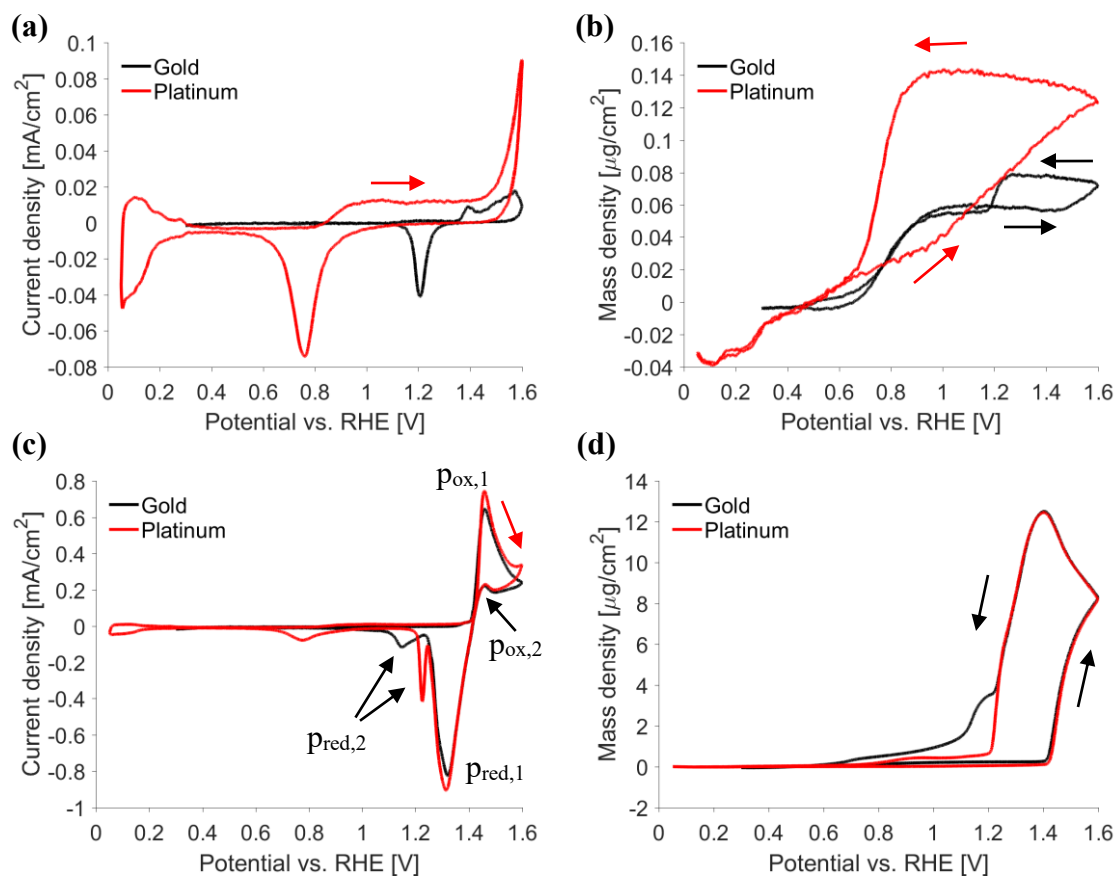

Figure 1. Cyclic voltammograms of gold (black line) and platinum (red line) electrodes in a) 0.1 M H_2SO_4 and c) 0.1 M H_2SO_4 + 5 mM $MnSO_4$ at sweep rate 5 mV/s. The corresponding massograms are shown in b) and d), respectively. Arrows not pointing at the peaks indicate sweep direction.

It is clear that the oxidation and reduction peaks appearing upon addition of Mn^{2+}-ions to the electrolyte are related to reactions involving manganese species. The second reduction peak ($p_{red,2}$) on the gold electrode does overlap with the reduction of gold oxide, but gold oxide reduction only contributes to 10 % of the charge passed in the peak at 5 mV/s, as also observed in (15).

The shape and size of the main oxidation peak ($p_{ox,1}$) and the first reduction peak ($p_{red,1}$) are very similar on both substrates, implying that the reactions occurring are independent of substrate. This is supported by the fact that the massograms of gold and platinum are similar in the same potential range (Figure 1d). The second reduction peak ($p_{red,2}$) is however dependent on the substrate. These results are in accordance with the findings of Lee *et al.* and Maskell (10-12) who found that the first reduction peak of electrodeposited MnO_2 was independent on the substrate, whereas the second peak was not.

The massograms and voltammograms of gold obtained in this work are qualitatively similar to those obtained by Devaraj and Munichandraiah (20) for the same experimental conditions. These authors observed a net increase in mass during potential cycling, which was on occasions observed in this work as well. However, since the voltammograms of gold in 0.1 M H_2SO_4 in reference (20) appear to be quite distorted as compared to those of other works (25), any further comparison is difficult.

Effect of sweep rate. The cyclic voltammograms and massograms of gold and platinum electrodes in manganese-containing electrolyte are shown for a number of sweep rates in Figure 2 and Figure 3, respectively. The peak current in the forward oxidation peak ($p_{ox,1}$) does not show a clear dependence on the sweep rate with a peak potential being shifted to more positive potentials with increasing sweep rates (Figure 2a and Figure 3a). Similar peak current trends with sweep rates were observed by Nijjer (26) at comparable conditions. However, at higher manganese concentration and elevated temperature Rodrigues *et al.* (16) found the peak current to be proportional to the square root of sweep rate indicating diffusion limitations at these conditions. Furthermore, the small oxidation peak observed in the reverse scan is clearly visible for the slower sweep rates, but exists only as a change in slope for the faster sweep rates. The oxidation peaks are discussed in more details later on in the reaction mechanism section.
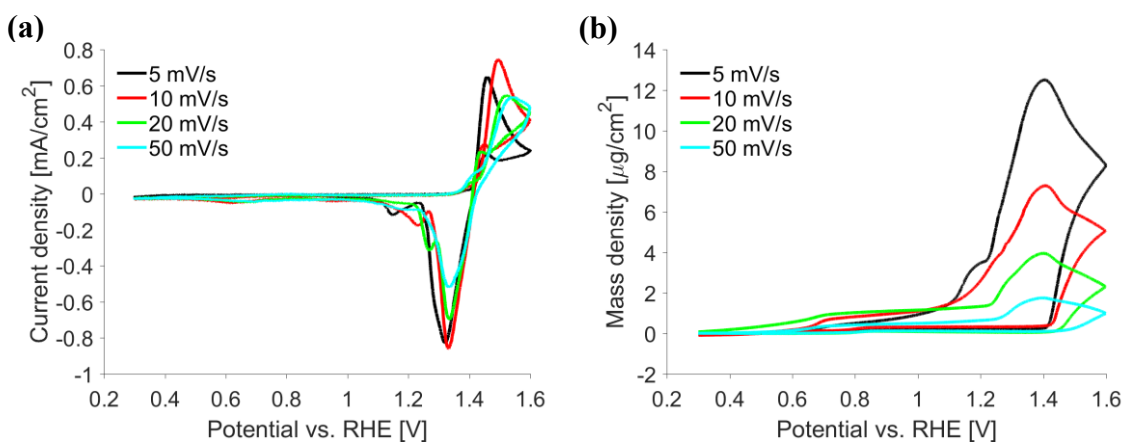
(a)

(b)

Figure 2. Cyclic voltammograms (a) and massograms (b) of a gold electrode in 0.1 M H_2SO_4 + 5 mM $MnSO_4$ at various sweep rates.
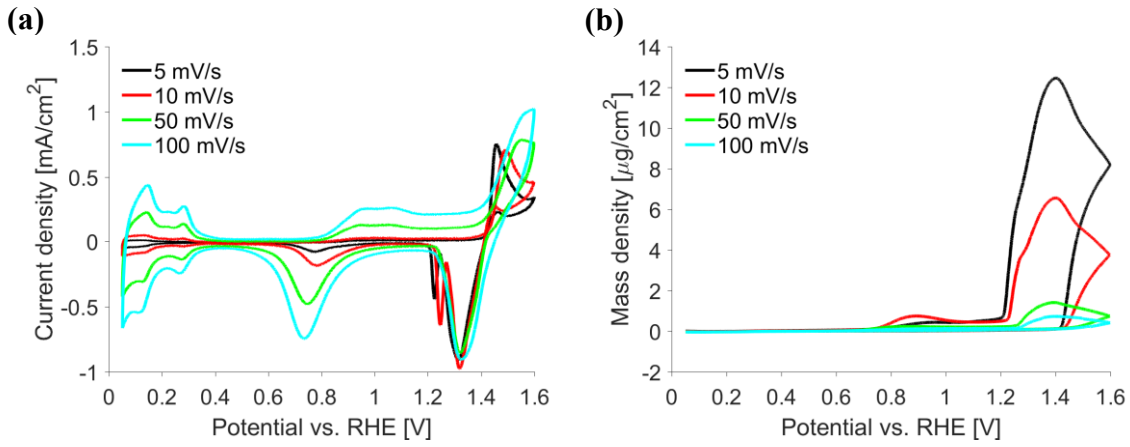
Figure 3. Cyclic voltammograms (a) and massograms (b) of a platinum electrode in 0.1 M H$_2$SO$_4$ + 5 mM MnSO$_4$ at various sweep rates.

The massograms in Figure 2b) and Figure 3b) show that the total mass deposited during one cycle was found to be inversely proportional to the sweep rate for the platinum electrode (proportional to $v^{-1.06}$) and not entirely so for the gold electrode (proportional to $v^{-0.88}$), although similar trends where observed.

The first reduction peak (p$_{red,1}$) displayed a significantly different behavior than the oxidation peak (p$_{ox,1}$), the salient feature being an independence of the peak current on sweep rate, especially prominent for the platinum electrode. This is expected since the peak current is proportional to both the sweep rate and the amount of deposited material for the reduction of a species deposited at an electrode, given by Eq. [13] for the reversible case and Eq. [14] in the irreversible case (27):

$$i_p = \frac{n^2 F^2}{4RT} v A \Gamma_O^*$$ [13]

$$i_p = \frac{\alpha F^2 v A \Gamma_O^*}{2.718 RT}$$ [14]

where i_p is the peak current, A the area, R the universal gas constant, F the Faraday constant, n the number of electrons transferred, v the sweep rate, α the transfer coefficient and Γ_O^* the initial amount of adsorbed oxidized species (O). Since the amount of deposited material formed in the oxidation sweep is inversely proportional to the sweep rate at the platinum electrode, $\Gamma_O^* \propto v^{-1}$, the product of these quantities results in a peak current independent of sweep rate. As mentioned above, the mass deposited at the gold electrode was not inversely proportional to the sweep rate. This explains why the peak current is observed to diminish as the sweep rate increases at the gold electrode, since the amount deposited at high sweep rate is less per time than at slower sweep rates.

The independence of the peak potential (p$_{red,1}$) on the sweep rate suggests that the reduction of the small amounts of manganese oxide deposit reduced in this reduction wave can be considered reversible (27).

A second reduction peak (p$_{red,2}$) was only observed at the lower sweep rates (20 mV/s and below) for both electrodes. This peak shifted negatively with decreasing sweep rate, *i.e.* as the deposit thickness increased due to increased time in the positive current region.

Effect of upper reversal potential. Here, the upper reversal potential was varied from 1.39 V prior to the rising part of the oxidation peak to 1.7 V, which is well above the peak (Figure 4). When looking more closely at the current response upon reversing the potential in the rising part of the voltammogram prior to the apex (*i.e.* below 1.46 V, Figure 4c), it is apparent that the current continued to rise even after the potential reversal. This is a clear indication of the nucleation, growth and collision mechanism expected in the deposition process of manganese oxide. In the reverse scan, only one reduction peak is observed at these potentials, although a shoulder can be seen at slightly more positive potentials.
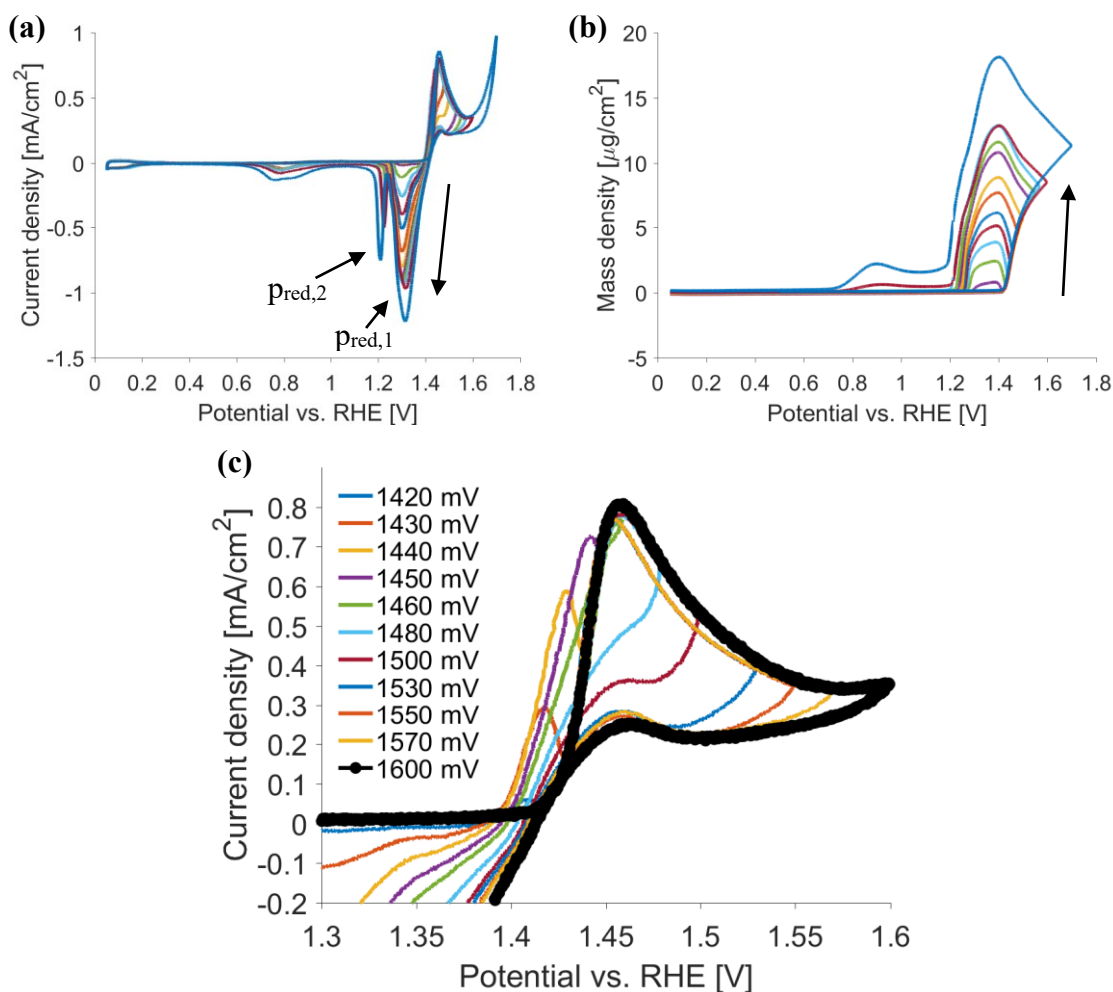

Figure 4. Cyclic voltammograms (a) and massograms (b) for a number of anodic reversal potentials ranging from 1.39 V to 1.7 V recorded at 5 mV/s on a platinum electrode in 0.1 M H_2SO_4 + 5 mM $MnSO_4$. The arrows indicate increasingly positive anodic reversal potentials. A magnification of the oxidation peaks for selected anodic reversal potentials is shown in (c) with the curve at 1.6 V emphasized in black.

Upon increasing the upper reversal potential beyond the apex, an oxidation peak appeared in the reverse scan ($p_{ox,2}$, Figure 1c) in addition to a transition from one to two reduction peaks (Figure 4a). The first peak ($p_{red,1}$) was observed at around 1.3 V increasing in size and with the disappearance of the small shoulder when the upper

reversal potential was increased. The second reduction peak ($p_{red,2}$) was only observed when the upper reversal potential was sufficiently positive, starting at 1.53 V on gold and 1.55 V on platinum. Furthermore, the second reduction peak became more significant and was shifted towards more negative potentials with an increasing upper reversal potential.

Figure 4b) illustrates the continuous increase in mass at potentials above the onset of manganese oxide formation and the varying reduction waves observed depending on upper reversal potential in accordance with the voltammograms.

The mass change obtained from EQCM can be compared with the measured current when considering Faraday's law as shown in Eq. [15]:

$$\frac{\mathrm{d}\Delta m_{\mathrm{EQCM}}}{\mathrm{d}t} = \frac{\mathrm{d}}{\mathrm{d}t}\left(\frac{\int I\ \mathrm{d}t}{nF} M \right) = \frac{M}{nF} I \qquad [15]$$

Thus, the time derivative of the mass change ($\mathrm{d}\Delta m/\mathrm{d}t$) is proportional to the measured current (I) assuming a constant number of electrons transferred (n), a constant molar mass of the deposit (M) and that the measured frequency change is governed solely by the electrodeposited species. This correlation is given in Figure 5 for the upper reversal potential of 1.6 V.
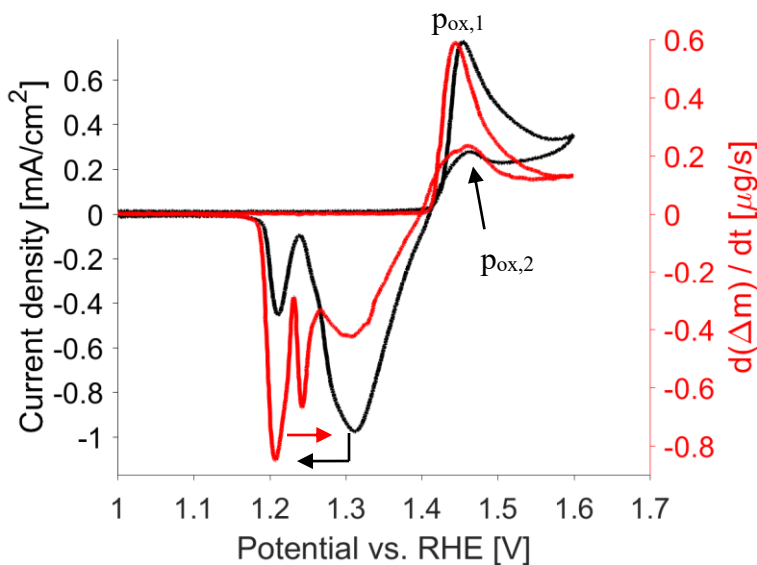

Figure 5. Cyclic voltammogram (black, left axis) and time derivative of mass from EQCM (red, right axis) for a platinum electrode in 0.1 M H_2SO_4 + 5 mM $MnSO_4$ at 5 mV/s showing the anodic region.

Both oxidation peaks showed a good correlation between the current and the time derivative of mass. The difference between the current and time derivative of mass at the most positive potentials is probably due to some oxygen evolution at these potentials, which contributes to the measured current, but not to the mass. Also, the mass is seen to increase slightly prior to the onset of oxidation current leading to ($p_{ox,1}$), perhaps indicating an adsorption process prior to the oxidation and formation of manganese deposit.

For the main part of the first reduction peak ($p_{red,1}$) more charge was passed than the mass signal indicated if assuming a two electron reduction of MnO_2 to Mn^{2+}. However, towards the end of the peak a shoulder was observed in the current signal that coincided with a considerable mass loss. This feature appeared for all upper reversal potentials. For cases in which the second reduction peak ($p_{red,2}$) was present, a higher mass loss than predicted was observed during this reduction.

Chronoamperometry

Chronoamperometric data were collected at potentials on each side of the apex (1.465 V) of the oxidation peak observed in the cyclic voltammograms ($p_{ox,1}$, Figure 1c). Initial experiments showed that the charge passed during chronoamperometric experiments first increased during the oxidation peak, but experienced a minimum at even more positive potentials (around 1.5 V) before increasing once more. Based on this, three potentials were selected (1.45 V, 1.50 V and 1.55 V) and the measured current and mass responses are presented in Figure 6. The potentials 1.45 V and 1.55 V were selected since they possess similar steady state currents while representing potentials at both sides of the apex. The current transients are similar with the exception of the nucleation and growth signature at shorter times at 1.45 V on both substrates (Figure 6a). This is not observed at the higher potentials perhaps due to the rather coarse time resolution used.

Interestingly, although the overall charge passed was found to be similar, the accumulated mass observed at the lower potential (1.45 V) was found to be significantly higher than that at the more positive potentials (1.50 V and 1.55 V) (Figure 6b). This demonstrates that the contribution to the oxidation current is different at either side of the apex. Figure 6c compares the deposited mass as a function of charge with the theoretical mass increase of MnOOH (n = 1) MnO_2 (n = 2) for the recorded current and mass transients. From this figure it is apparent that more charge is needed to produce a given amount of mass at higher potentials. In fact, the mass density vs accumulated charge density matches the theoretical line of MnO_2 formation at 1.55 V. Conversely, at 1.45 V the slope lies in between those of MnO_2 and MnOOH indicating an incomplete oxidation to MnO_2. A slope in between that of MnOOH and MnO_2 was also observed by Dupont and Donne during at 1.3 V vs. SCE with higher manganese concentration (9).

Diffusion characteristics such as Cottrell behavior in the current transients were not observed, in agreement with the independence of the peak current on sweep rate (Figure 2 and Figure 3). This is in contrast to that observed by Dupont and Donne at long times (over 30 s) (9). However, at such long times natural convection may start to influence the measured current (27) and any differences in cell geometry could play a significant role.
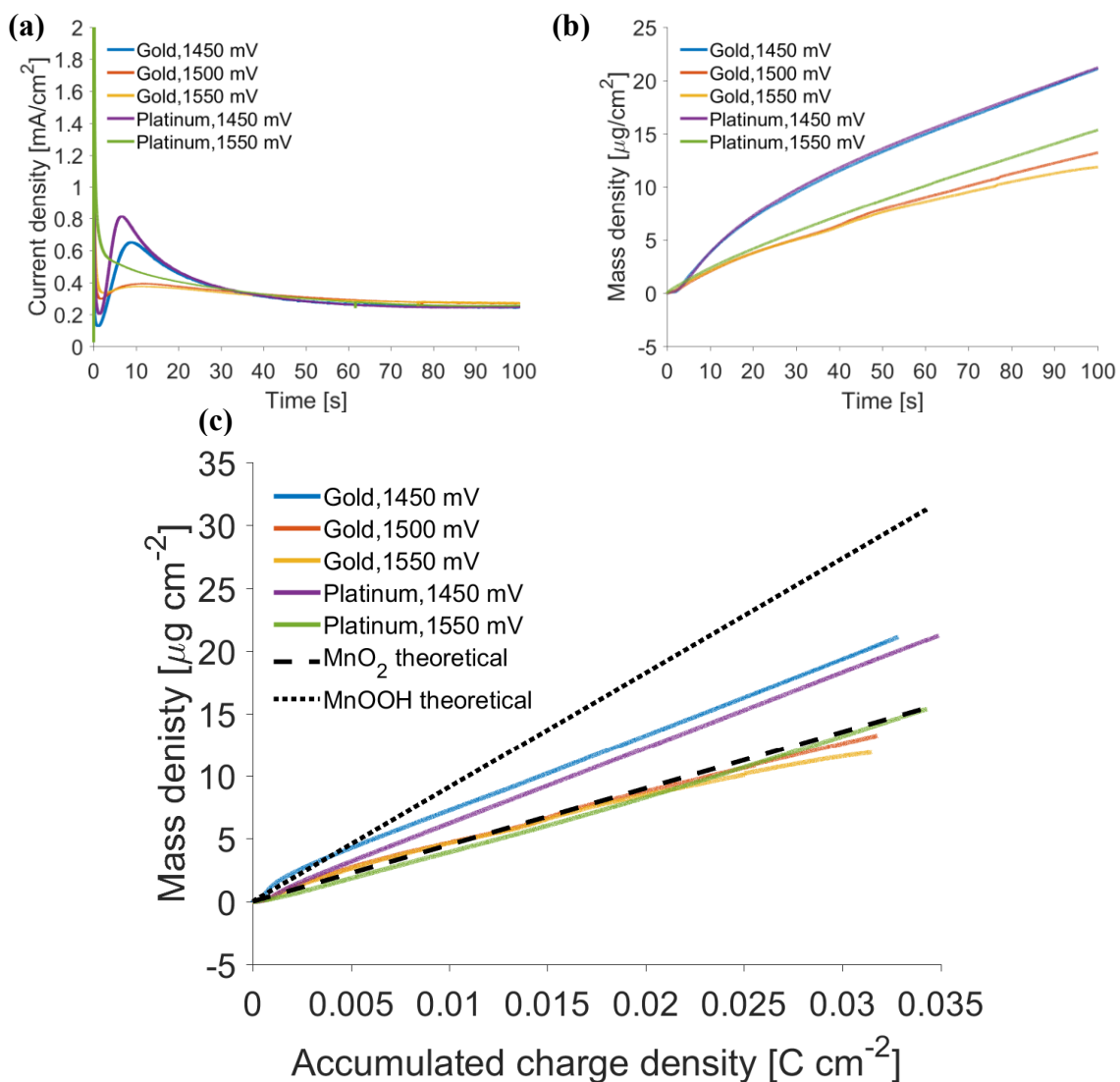
Figure 6. Current transients (a) and mass transients (b) for potential steps on platinum and gold electrodes in 0.1 M H_2SO_4 + 5 mM $MnSO_4$. A different representation of the same experiments are shown in (c) where the mass density calculated from the frequency is plotted versus the accumulated charge calculated from the current. The theoretical development for MnO_2 and $MnOOH$ formation are also included.

Negative-going linear sweeps were initiated immediately after the chronoamperometric experiments, from Figure 6, to investigate the manganese oxide being formed at the selected potentials from the accompanying reduction processes (Figure 7). Similarly, a positive-going sweep was initiated after a sweep-hold experiment for 100 s at 1.45 V (Figure 8). In both cases, there are a number of reduction peaks occurring in the first negative-going sweep where shape, size and position depend on hold potential, hold time, sweep direction and substrate, analogous to what was observed when varying the upper reversal potential (Figure 4). This indicates a more complicated reduction scheme during the first negative-going scan than the subsequent sweeps, resembling the familiar features from conventional voltammograms (Figure 8, cycle 2).
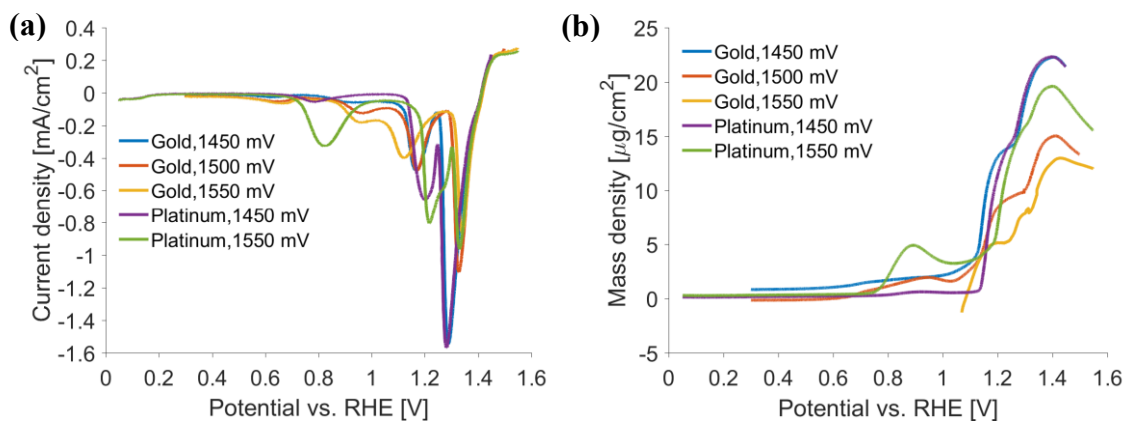
Figure 7. Linear sweep voltammetry (a) at 5 mV/s following chronoamperometric experiments for 100 s at a number of potentials in 0.1 M H_2SO_4 + 5 mM $MnSO_4$. The corresponding mass responses are given in (b).
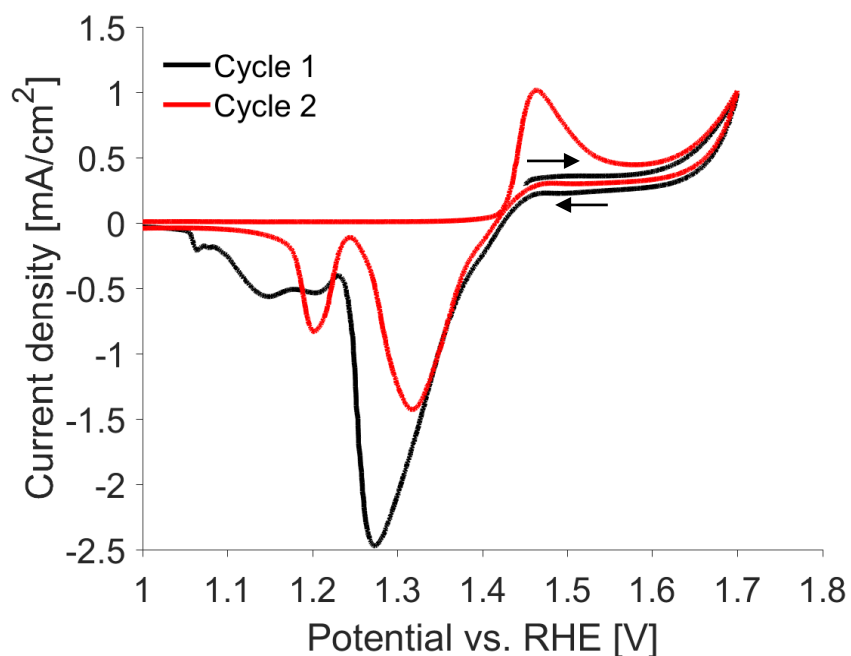

Figure 8. Two subsequent cycles at 5 mV/s after sweep-hold for 100 seconds at 1.45 V in the positive-going sweep on a platinum electrode in 0.1 M H_2SO_4 + 5 mM $MnSO_4$. Initial scan direction after the hold was positive.

Clearly, the first reduction peak ($p_{red,1}$) includes a larger current in the first negative-going sweep from 1.45 V than from higher potentials (Figure 7a), including a shift of the peak potential to more negative potentials. Furthermore, the mass decrease was considerably larger during the second peak than the first peak for all potentials, similarly to that observed in Figure 5.

Scanning Electron Microscopy

The manganese oxide deposits obtained from chronoamperometric experiments on platinum discs were imaged with SEM (Figure 9). After withdrawal of the electrode from the electrolyte, the wet deposit appeared to be continuous and uniform by visual inspection. However, the deposit cracked and crumpled up upon drying and in most cases detached to a large degree from the surface, as can be observed in the micrographs. From the images after 1000 s and 10 000 s it is clear that the amount of dendrites formed during deposition was larger at 1.55 V than at 1.45 V, indicated by red arrows in Figure 9e) and f).

Interestingly, the thickness of the deposit obtained at 1.45 V was less than that at 1.55 V after 10 000 s (Figure 9c and f). The charge passed during deposition was similar for the two films, although somewhat higher at 1.55 V in this case (in contrast to Figure 6). The higher thickness but lower expected mass (Figure 6b) indicates a higher porosity of the film formed at 1.55 V. As mentioned above, the EQCM measurements suggest different deposits at the two potentials, MnO_2 at 1.55 V and a mixture of MnO_2 and $MnOOH$ at 1.45 V, likely to be the main reason for the different porosity observed.
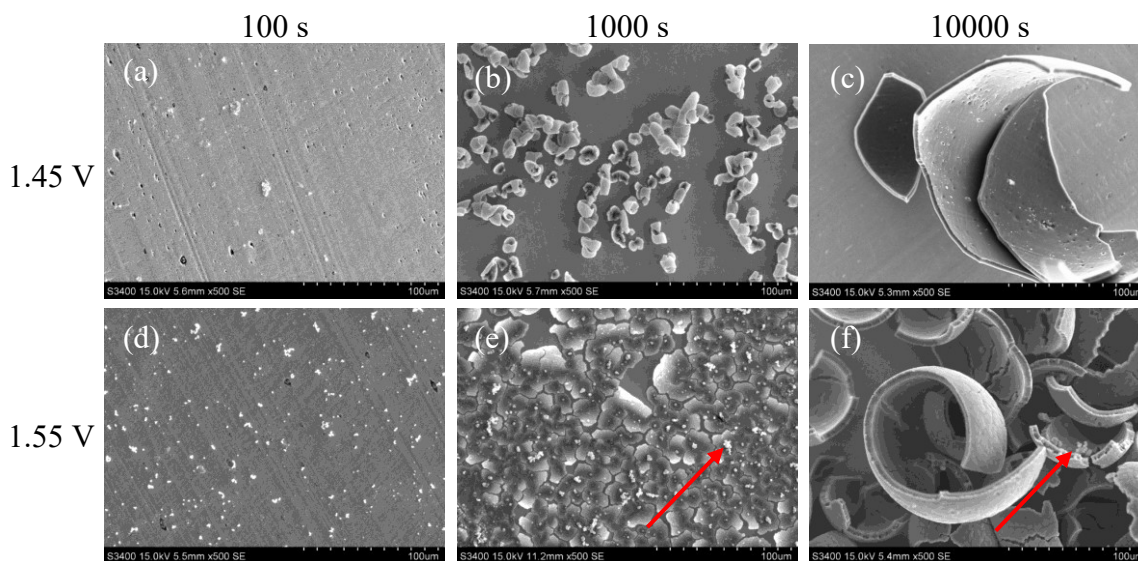

Figure 9. SEM micrographs of manganese oxide deposits obtained at different deposition potentials and times in 0.1 M H_2SO_4 + 5 mM $MnSO_4$, 500X magnification.

Reaction mechanisms

Oxidation processes. A satisfactorily reaction mechanism for the oxidation processes must satisfy the main experimental observations on both gold and platinum. An ECE mechanism given by Equations [1]-[3] has been suggested by Petitpierre et al. (5). In this work, we assume a similar mechanism where manganese oxide deposition occurs initially at a noble metal oxide (Au or Pt) covered surface through a nucleation growth and collision mechanism. Signatures of a nucleation growth and collision mechanism were clearly seen in the sweep-reversal experiments (Figure 4c), chronoamperometry (Figure 6a) as well as in sweep-hold experiments. The oxidation peak in the positive going sweep ($p_{ox,1}$, Figure 1c) can thus be explained if the adsorption of Mn^{2+} and oxidation to Mn^{3+}

are confined to the perimeter of growing islands of manganese deposits at the surface. The active area, and hence the current, will then initially increase due to the growing islands until they collide and combine, which reduces the active area.

Previously, the oxidation peak during manganese oxide deposition ($p_{ox,1}$) has been explained in terms of the poor electrical conductivity of MnOOH, which would result in a reduction of the current when the metal surface is fully covered (7) and by diffusion yielding a Cottrell behavior (9, 16).

Furthermore, EQCM measurements from the chronoamperometry experiments (Figure 6) indicate that the oxidation product at a high potential (1.55 V) was MnO_2, whereas at a lower potential (1.45 V) a mixture between MnO_2 and MnOOH was produced. These results are in accordance with the ECE mechanism where MnOOH is formed at lower potentials (Eqs. [1] and [2]) and is further oxidized to MnO_2 at higher potentials (Eq. [3]). Some MnO_2 is formed at the lower potential as well, but the kinetics of reaction [3] might not be sufficient to convert all the formed MnOOH to MnO_2. In addition, the MnO_2 formed at the lower potential might originate from the disproportionation mechanism given by Equations [1], [4] and [5]. This mechanism can be expected to be more prominent at lower pH due to the increased stability of the Mn^{3+}-ion (9).

Estimating the charge involved in the manganese oxide formation prior to the peak in the voltammograms ($p_{ox,1}$) can give an indication of whether the manganese oxide deposits grow in-plane with the surface to form one monolayer (ML) or grow in a three-dimensional shape (e.g. suppressed hemispheres) yielding several MLs worth of charge before they coalesce and the area reduces. The active area of a Pt electrode can be estimated by assuming that the charge under the hydrogen underpotential deposition peaks corresponds to 220 $\mu C/cm^2$ (one charge per surface Pt atom). Thus, from Figure 1c) and Figure 3a) and assuming maximum one electron transfer per Pt surface atom (Eqs. [1]-[2]) formation of one ML of MnOOH can expected to be at 1.44 V at 5 mV/s. This is in the rising part, prior to the peak, and most likely the saturation coverage is less than one charge per surface Pt, which then occurs at even lower potentials. We can therefore assume that three-dimensional islands of manganese deposits are being formed in the nucleation and growth stage.

The second oxidation peak ($p_{ox,2}$) that occurs in the negative-going sweep at low sweep rates (Figure 1c) coincides with the oxidation peak in the positive-going sweep ($p_{ox,1}$), but cannot be explained in terms of a nucleation and growth mechanism. It cannot be explained as a superposition of reduction and oxidation reactions either, or else the CV and the massogram should not have overlapped as they do in Figure 5. Any reduction through Eq. [6] during the peak would lead to a slight increase in mass but a cathodic contribution to the current, and result in a discrepancy between current and the time derivative of mass.

The second oxidation peak also appeared during negative-going sweeps on thicker deposits, although not so strong (e.g. Figure 8). In order to explain this oxidation peak we need an additional aspect to the oxidation processes. MnOOH possesses a lower conductivity than MnO_2 (7, 14, 28). Here we propose that the adsorption and oxidation of Mn^{2+} to form MnOOH is more likely to happen on MnOOH than on MnO_2 at a given potential. Furthermore, the limited electrical conductivity through MnOOH efficiently restricts the growth of MnOOH dendrites. At low potentials, a large fraction of the surface is MnOOH in comparison to higher potentials, where the oxidation to MnO_2 is considered to be fast with low amounts of MnOOH available. This can suggest a more efficient oxidation at lower potentials yielding more deposit at low potentials in

comparison to high potentials and an even current distribution leading to more even and denser deposits. This is also what we observe in the EQCM measurements (Figure 6) as well as cross-sections of the deposits obtained after 10000 s (Figure 9).

Based on the considerations above, the peak potential shift of the positive-going oxidation peak ($p_{ox,1}$) to more positive potentials at increasing sweep rates but with less accumulated charge could be understood as a delay of adsorption and oxidation of Mn^{2+} at higher sweep rates. Furthermore, the higher potentials increase the rate of transformation of MnOOH to MnO_2 further limiting the reaction leading to slower growth.

Reduction processes. From the voltammograms and massograms obtained in this work it is clear that the reduction behavior is complex and very dependent on key parameters such as the deposition potential, sweep rate and the resident time as well as electrode substrate. Sweep-reversal and sweep-hold experiments during the first oxidation peak show the transition from one reduction peak ($p_{red,1}$) alone to the existence of a second ($p_{red,2}$) or more reduction waves. The first reduction peak ($p_{red,1}$) was found to be larger at low deposition potentials in comparison to at higher deposition potentials (Figure 7) indicating that the manganese deposit formed at lower potentials was somehow easier to reduce.

The reduction behavior can be explained by the mechanism given by Lee *et al*. and Maskell (10-12) in Eqs. [6] and [7]. According to these authors, the second reduction peak emerges due to an increase in contact resistance from a volume reduction leading to a decrease in conductivity of the remaining deposit. This could explain why a thicker deposit or a deposit with higher porosity (typically stemming from deposition at higher potentials) are harder to remove, as observed in this work. As the deposition procedure increased in duration and complexity the reduction peaks are more abstruse (*i.e.* Figure 8; long hold time and sweeping to oxygen evolution first) perhaps indicating local variations in deposit properties and current distribution leading to multiple reduction waves.

Furthermore, the proposed reduction mechanism can explain the discrepancies between the current and the time derivative of mass observed in main part of the first reduction peak ($p_{red,1}$) in Figure 5. The observed decrease in mass was smaller than expected from a direct reduction from either MnO_2 or MnOOH to Mn^{2+}-ions. The first reduction peak can neither be ascribed solely to reaction [6] without any following chemical or electrochemical reaction as suggested by some authors (16, 20). This would have resulted in a slight mass increase contrary to what was observed. Hence, a combination of an electrochemical reduction reaction giving a slight increase in mass (Eq. [6]) with a following chemical reaction giving a mass decrease (Eq. [7]) can explain the experimental observations.

Towards the end of the first reduction peak ($p_{red,1}$), a sharp mass increase was observed (Figure 5), showing that the peak labeled as $p_{red,1}$ might actually be two overlapping reduction peaks. If most of the MnO_2 was converted to MnOOH during the main part of the first reduction peak (Eq. [6]), two neighboring MnOOH species needed for reaction [7] to proceed would occur more frequently. Hence, the speed of reaction [7] might increase leading to the observed sharp mass decrease. A direct reduction of MnOOH through Equation [8] would have caused a large mass decrease, but a charge corresponding to a one-electron transfer reaction should have been observed simultaneously. The charge passed in this region of the voltammogram seems too low compared with the mass change to be consistent with a reduction solely through reaction [8]. A combination of reactions [7] and [8] is however a possibility.

The second reduction peak ($p_{red,2}$) showed a similar behavior as the last part of the first reduction peak with more mass change than predicted from the charge passed. The same considerations as given in the previous paragraph thus apply for this reduction peak as well.

Chemical reactions resulting in solution free species such as reactions [9] or [10] could lead to a mass loss without any observed reduction peak. However, the Mn^{3+}-ion is not very stable in the weakly acidic electrolyte and would either hydrolyze or disproportionate as seen in the positive-going sweep leading to an increase in mass or be reduced to Mn^{2+} through reaction [11] giving a reduction current. Hence, these reactions do not explain the discrepancies between mass loss and current as observed in Figure 5.

It is worth pointing out that we have not considered the influence of water intrusion into the deposit in our interpretation, which would be included in the signal from the EQCM and possibly somewhat distort the observed mass loss.

Conclusion

The observed behavior during manganese oxide deposition was described by an ECE mechanism where MnOOH is formed in the chemical step and is further oxidized to MnO_2 at higher potentials. By comparing the mass from the EQCM and the charge, the product of Mn^{2+} oxidation was found to be a mixture of MnOOH and MnO_2 at a lower potential (1.45 V), whereas at a higher potential (1.55 V) a full conversion to MnO_2 was observed. A nucleation and growth mechanism was observed during the initial stages of deposition with a suggested three-dimensional growth of the nuclei. The initial stages of the deposition process (adsorption and oxidation of Mn^{2+} to form MnOOH) was proposed to be faster on MnOOH than on MnO_2, giving a faster deposition rate and denser deposit at lower potentials.

The reduction was found to be complex, depending particularly on the thickness of the deposit. A reduction mechanism was proposed to involve an electrochemical reduction of MnO_2 to MnOOH followed by a chemical reaction yielding Mn^{2+} and MnO_2. It was found that the reduction could not occur solely through two consecutive electrochemical steps.

Acknowledgments

References

1. M. Pourbaix, *Atlas of electrochemical equilibria in aqueous solutions*, Pergamon Press, Oxford (1966).
2. T. N. Andersen, in *Modern aspects of electrochemistry: 30*, R. E. White, Editor, p. 313, Plenum Press, New York (1996).

3. R. L. Paul and A. Cartwright, *J. Electroanal. Chem. Interfacial Electrochem.,* **201**, 113 (1986).
4. R. L. Paul and A. Cartwright, *J. Electroanal. Chem. Interfacial Electrochem.,* **201**, 123 (1986).
5. J. P. Petitpierre, C. Comninellis, and E. Plattner, *Electrochim. Acta,* **35**, 281 (1990).
6. J. Y. Welsh, *Electrochem. Technol.,* **5**, 504 (1967).
7. S. Nijjer, J. Thonstad, and G. M. Haarberg, *Electrochim. Acta,* **46**, 395 (2000).
8. G. Davies, *Coordin. Chem. Rev.,* **4**, 199 (1969).
9. M. F. Dupont and S. W. Donne, *Electrochim. Acta,* **120**, 219 (2014).
10. J. A. Lee, W. C. Maskell, and F. L. Tye, *J. Electroanal. Chem. Interfacial Electrochem.,* **79**, 79 (1977).
11. J. A. Lee, W. C. Maskell, and F. L. Tye, *J. Electroanal. Chem. Interfacial Electrochem.,* **110**, 145 (1980).
12. W. C. Maskell, *J. Electroanal. Chem. Interfacial Electrochem.,* **199**, 127 (1986).
13. S. Bodoardo, J. Brenet, M. Maja, and P. Spinelli, *Electrochim. Acta,* **39**, 1999 (1994).
14. P. Ruetschi and R. Giovanoli, *J. Electrochem. Soc.,* **135**, 2663 (1988).
15. Z. Rogulski, H. Siwek, I. Paleska, and A. Czerwiński, *J. Electroanal. Chem.,* **543**, 175 (2003).
16. S. Rodrigues, N. Munichandraiah, and A. K. Shukla, *J. Appl. Electrochem.,* **28**, 1235 (1998).
17. S. Nijjer, J. Thonstad, and G. M. Haarberg, *Electrochim. Acta,* **46**, 3503 (2001).
18. D. Gosztola and M. J. Weaver, *J. Electroanal. Chem. Interfacial Electrochem.,* **271**, 141 (1989).
19. A. D. Cross, A. Morel, M. Drozd, I. Olcomendy, A. F. Hollenkamp, and S. W. Donne, *Electrochim. Acta,* **87**, 133 (2013).
20. S. Devaraj and N. Munichandraiah, *Electrochem. Solid-State Lett.,* **12**, F21 (2009).
21. M. P. Owen, G. A. Lawrance, and S. W. Donne, *Electrochim. Acta,* **52**, 4630 (2007).
22. D. A. Buttry and M. D. Ward, *Chem. Rev.,* **92**, 1355 (1992).
23. V. I. Birss, M. Chang, and J. Segal, *J. Electroanal. Chem.,* **355**, 181 (1993).
24. Z. Jusys and S. Bruckenstein, *Electrochem. Solid-State Lett.,* **1**, 74 (1998).
25. R. Woods, in *Electroanalytical Chemistry*, A. J. Bard, Editor, Marcel Dekker, New York (1976).
26. S. Nijjer, *Deposition and reduction of manganese dioxide on alternative anode materials in zinc electrowinning*, NTH, Trondheim (2000).
27. A. J. Bard and L. R. Faulkner, *Electrochemical Methods: Fundamentals and Applications*, 2nd ed, p. 591, Wiley, New York (2001).
28. W. H. Kao and V. J. Weibel, *J. Appl. Electrochem.,* **22**, 21 (1992).